# Ultrahigh Pressure Equation of State of Tantalum to 310 GPa

Kaleb C. Burrage[1], Christopher S. Perreault[1], Eric K. Moss[2], Jeffrey S. Pigott[2], Blake T. Sturtevant[2], Jesse S. Smith[3], Nenad Velisavljevic[3,4], Yogesh K. Vohra[1*]

[1]Department of Physics, University of Alabama at Birmingham, Birmingham, AL 35294, USA
[2]Shock and Detonation Physics Group (M-9), Los Alamos National Laboratory, Los Alamos, NM 87545, USA
[3]High Pressure Collaborative Access Team, X-ray Science Division, Argonne National Laboratory, Argonne, IL 60439, USA
[4] Physics Division, Physical & Life Sciences Directorate, Lawrence Livermore National Laboratory, Livermore, CA, 94551, USA
[*] Corresponding author: ykvohra@uab.edu

**Abstract**

The isothermal compression of transition metal tantalum (*Ta*) was studied in a diamond anvil cell by x-ray diffraction utilizing rhenium (*Re*) and gold (*Au*) as internal x-ray pressure standards. The *Re* pressure marker was employed during non-hydrostatic compression to pressures up to 310 GPa while the *Au* pressure marker was used during quasi-hydrostatic compression in a neon pressure-transmitting medium to 80 GPa. Two ultra-high pressure experiments were conducted on *Ta* and *Re* mixtures utilizing focused-ion beam machined toroidal diamond anvils with central flats varying from 8 microns to 16 microns in diameter. The *Ta* metal was observed to be stable in the body-centered-cubic phase to a volume compression $V/V_0 = 0.581$. The measured equations of state (EOS) of *Ta* using two different calibrations of the *Re* pressure marker are compared with the ambient temperature isotherm derived from shock compression data. We provide a detailed analysis of EOS fit parameters for *Ta* under quasi-hydrostatic and non-hydrostatic conditions.

## INTRODUCTION

The generation of near-terapascal (TPa, 1 TPa = 1000 GPa) static pressures in diamond-anvil cell devices has necessitated a search for reliable x-ray pressure standards and research on cross-comparison of pressure standards for use in studies of materials under extreme conditions. In general, rhenium (*Re*) is used extensively as a gasket material in high-pressure diamond cell experiments, and also serves as an internal x-ray pressure standard. The 5d transition metal tantalum (*Ta*) is expected to be stable in the body-centered-cubic phase to multi-megabar pressures and offers an opportunity for cross-comparison with other pressure standards like *Re*. The use of nanocrystalline diamond (NCD) micro-anvils as pressure generators in traditional single-stage diamond anvil cell devices has received extensive attention recently as earlier studies have raised the prospect of achieving TPa static pressure in the laboratory[1-3]. There have been two distinct approaches in the fabrication of NCD micro-anvils: the first approach is to convert glassy carbon into NCD micro-ball by the application of high pressure and high temperatures[1], and the second approach has been to directly deposit NCD diamond on an existing anvil by combining mask-less lithography and chemical vapor deposition (CVD)[4-6]. Even though both approaches have shown the ability to generate ultra-high pressures, direct CVD growth of NCD on existing diamond anvil offers advantages in terms of alignment and reproducibility in generation of ultra-high static pressures. In parallel, there have been developments in generating ultra-high pressures by employing focused-ion beam (FIB) shaping to fabricate micro-anvils from single crystal diamond as well as nano-polycrystalline diamond (NPD)[7-9]. Very recently, FIB has been utilized to fabricate toroidal diamond anvils to achieve a pressure of ~600 GPa on a *Re* gasket[10-11]. These toroidal diamond anvils are designed to circumvent problems associated with the large elastic deformation experienced by diamond at multi-megabar pressures. Additionally, discrepancies in the *Re* equation of state[9,12] have been exposed at extreme pressures and a new equation of state (EOS) for Re has been proposed for use in the multi-megabar regime[12]. It should be added that this new EOS of *Re* has been calibrated to 144 GPa[12] using a variety of pressure markers like ruby, helium pressure medium, and tungsten. The present high-pressure study is motivated by the use of *Re* as an x-ray pressure standard in the measurement of the equation of state of *Ta* to multi-megabar pressures. The equation of state of *Ta* thus obtained with the two different EOS for *Re* is compared with the room temperature isotherm derived from shock compression data. In addition, we also

examine the differences between the equation of state of *Ta* measured under both quasi-hydrostatic and non-hydrostatic pressure conditions. The ultra-high pressure studies on *Ta* have been carried out using toroidal anvils with central flats ranging from 8 microns to 16 microns in diameter and micro x-ray diffraction studies performed at high-pressures using a synchrotron source.

**EXPERIMENTAL**

The toroidal anvils in this study were prepared by ion-beam milling of single crystal diamond anvils by utilizing the Tescan Lyra3 FIB-SEM facility at the University of Alabama-Tuscaloosa's Central Analytical Facility. The starting diamond anvil was of beveled design with 25 micron central flat and 8 degree bevel to a culet of 300 microns in diameter. The FIB-milling of the diamond surface was done using a $Ga^{+}$-ion beam held at 5 nA and 30 keV with a beam size of 50 nm. The ultra-high pressure non-hydrostatic experiments in this study utilized two pairs of toroidal diamond anvils. The first pair of toroidal anvils had a central flat region of 16 microns and outer regions of 40 and 65 microns in diameter with a groove depth of 2.6 microns (Figure 1) and achieved a static pressure of 265 GPa. The second pair of toroidal anvils had a central flat region of 8 microns and outer regions of 20 and 35 microns in diameter with a groove depth of 5 microns (Figure 2) and achieved a static pressure of 310 GPa. Two matching anvils were made and employed in an opposing anvil configuration in a diamond anvil cell. For the toroidal DAC experiments, *Ta* (99.95% purity) and *Re* (99.97% purity) gaskets were made from Alfa Aesar polycrystalline foils. The gaskets were 25 microns each and overlaid between the two opposed anvils. Angle-dispersive x-ray diffraction experiments ($\lambda$ = 0.4066 Å) were conducted at the High Pressure Collaborative Access Team (HPCAT) beamline 16-ID-B of the Advanced Photon Source at Argonne National Laboratory. XRD patterns were recorded on a Pilatus 1M pixel array detector with a focused x-ray beam size of 1 μm (vertical) x 2 μm (horizontal) (FWHM) on sample in toroidal diamond anvils. The sample-to-detector distance (209.73 mm) was calibrated using $CeO_2$.

For quasi-hydrostatic compression using a neon pressure medium, a symmetric DAC equipped with a pair of 200 micron flat diamond anvils was loaded with ultra-high purity *Ta* from Los Alamos National Laboratory along with a small amount of gold powder which acted as a pressure standard[13]. As neon freezes to a solid at approximately 5 GPa at ambient temperature, we expect sample to develop some uniaxial strain and thus label this experiment as quasi-hydrostatic Angle-dispersive x-ray diffraction ($\lambda$ = 0.4246 Å) experiments were conducted at the HPCAT beamline

16-BM-D. The XRD patterns were collected on a Mar345 image plate with a focused x-ray beam size of 4 μm (vertical) x 5 μm (horizontal) (FWHM) The sample-to-detector distance (465.48 mm) was calibrated using $CeO_2$.

The software package Dioptas[14] was used to integrate the collected diffraction patterns, which were then analyzed using GSAS-II[15] structural refinement software. The following two equations of state are employed in this paper, the Rydberg-Vinet formulation[16] and the Birch-Murnaghan 4th Order EOS proposed for *Re*[3] as shown in equation (1) and (2) below with $x = V/V_0$, bulk modulus $K_0$, its first pressure derivatives $K'_0$, and its second pressure derivative $K''_0$.

$$P(V) = 3\,K_0\,x^{-2/3}(1 - x^{1/3})\exp\{1.5(K'_0 - 1) \times (1 - x^{1/3})\}. \quad (1)$$

$$P(V) = 3\,K_0\,f\,(1 + 2f)^{5/2}(1 + 1.5(K'_0 - 4)f + 1.5(K_0\,K''_0 + (K'_0 - 4)(K'_0 - 3) + 35/9)f^2) \quad (2)$$

$$f = ((V_0/V)^{2/3} - 1)/2 \quad (3)$$

The Re pressures were calculated based on two different methods and based on the volume $V$ and volume change ($V/V_0$) at high pressures, as determined from x-ray diffraction data. In the first method, equation of state parameters by Anzellini *et al*[12], i.e., bulk modulus $K_0$ = 352.6 GPa, its pressure derivative $K'_0$ = 4.56 along with equation (1) are used. Equation of state parameters by Dubrovinsky *et al*[3], $K_0$ = 342 GPa, $K'_0$ = 6.15 and $K''_0$ = -0.029 along with equation (2) and (3) are used in the second method. For precise determination of $V_o$, we independently measured the ambient pressure lattice parameters by x-ray diffraction for *Ta* and *Re* foil samples used in our experiments, for *Ta* is $a$ = 3.302±0.003 Å ($V_0$ (*Ta*) = 18.001 Å$^3$/atom) and for *Re* $a$ = 2.762±0.003 Å, $c$ = 4.461±0.005 Å ($V_0$ (*Re*) = 14.736 Å$^3$/atom).

**RESULTS**

Figure 3 (a) shows the integrated x-ray diffraction profiles for *Ta-Re* mixture in a toroidal diamond anvil at pressures of 265±10 GPa, where pressure is measured by the EOS of *Re*[12] using equation (1) with $K_0$ = 352.6 GPa and pressure derivative $K'_0$ = 4.56. Figure 3 (a) also shows the difference curve at the bottom after Rietveld refinement of structural parameters including a basal-plane texture for *Re*. Figure 3 (b) shows an X-ray diffraction image of the *Ta-Re* mixture at 265 GPa indicating spottiness or texturing for *Re* diffraction lines while the *Ta* diffraction lines are continuous. The *Ta* diffraction pattern is assigned to a body-cented-cubic (bcc) lattice as evidenced by (110), (200). (211), (220), and (310) diffraction peaks assigned to a cubic-phase at all pressures.

The *Re* diffraction pattern is assigned to a hexagonal-close-packed (hcp) lattice as evidenced by the (100), (101), (110), (200), (112), (201), (202), and (203) diffraction peaks assigned to a hexagonal lattice at all pressures. The (002) diffraction peak from *Re* is notably absent due to a basal-plane texture common for hcp metals under high pressure. This texturing in *Re* leads to the alignment of c-axis of the hexagonal grains perpendicular to the diamond culet or along the load-axis of the diamond anvil cell. The texture in *Re* was observed to persist to the highest pressure of 310 GPa. The refined lattice parameters in Figure 3 (a) at 265 GPa for *Ta*, $a = 2.787 \pm 0.008$ Å and for *Re* $a = 2.464 \pm 0.001$ Å, $c = 3.943 \pm 0.057$ Å. The measured lattice parameter yields a volume compression ($(V/V_0)_{Ta} = 0.601 \pm 0.025$) at 265 GPa. The body-centered-cubic phase of *Ta* is found to be stable to the highest pressure of 310 GPa. The measured lattice parameters at the highest pressure of 310 GPa are for *Re*: $a = 2.436 \pm 0.002$ Å, $c = 3.916 \pm 0.003$ Å with $(V/V_0)_{Re} = 0.683 \pm 0.007$ and for *Ta*: $a = 2.755 \pm 0.003$ Å with $(V/V_0)_{Ta} = 0.581 \pm 0.009$.

Figure 4 shows a 2-D x-ray transmission scan of the sample region at a pressure of 310 GPa for the toriodal anvil shown in Figure 2. This transmission scan covers a ± 20 micron region along the Y-axis and Z-axis that is perpendicular to the x-ray propagation along the X-axis. The maximum transmission indicated by a circle at the center in Figure 4 is the thinnest part of the sample and corresponds to the 8 micron central flat region of the toroidal anvil. The transmission decreases as one moves away from the center to the thicker part of *Ta* and *Re* sample and the transmission maintains a symmetric shape over the entire toroidal region of 35 microns in diameter (Figure 2). Figure 4 shows an increase in x-ray transmission intensity at the outer periphery ± 15 micron from the center of the toroidal anvil, thereby indicating thinning of gasket leading to diamond contact at the edge of the toroidal region. This is consistent with the diamond failure that is observed on increasing pressure beyond 310 GPa in this experiment.

Shown in Figure 5 is the resulting volume change during compression of *Ta* under quasi-hydrostatic conditions and calculated based on *Au* pressure standard[13] to 80 GPa. The experimental data points are fitted to the Rydberg-Vinet EOS[16] with the fit parameters summarized in Table 1. Likewise, Figure 6 shows the volume change in *Ta* under non-hydrostatic conditions to 310 GPa using *Re* as an internal pressure marker, with equation of state parameters given by Anzellini *et al*[12]. In Figure 6, open symbols are the experimental data points to the the highest volume

compression $V/V_0 = 0.581$ and the dashed curve is the Rydberg-Vinet EOS[16] with fit parameters summarized in Table 1 (labeled as Non-hydrostatic I).

**DISCUSSION**

All pressure-volume data from our measurement are shown in Figure 7 and and the resulting EOS fit parameters are summarized in Table 1. The shock EOS parameters are obtained by fitting the room-temperature pressure-volume data from Reference 17 to equation (1) and the values obtained are $K_0$ =189.4 GPa and $K'_0$ = 3.90. The earlier high pressure eqaution of state measurements on *Ta* were limited to a pressure of 174 GPa[18-19]. In Figure 7, we compare the equation of state measurements on *Ta* using pressure calculations with two different models of equation of state of *Re* (labeled as Non-hydrostatic I and Non-hydrostatic II). It is clear from Figure 7, that the Dubrovinsky *et al*[3] EOS, $K_0$ = 342 GPa, $K'_0$ = 6.15 and $K''_0$ = -0.029 used in conjunction with equation (2) significantly overestimates the pressure (Non-hydrostatic II). In fact, at the highest sample compression, pressure is 422 GPa based on Dubrovinsky *et al*[3] EOS and is only 310 GPa based on Anzellini *et al*[12] EOS. This is also reflected in the EOS fit of *Ta* which results in a very high value of $K'_0$ = 6.05 (Table 1, Nonhydrostatic II)) with fit clearly diverging from other curves in Figure 7. This overestimation of pressure in Dubrovinsky *et al*[3] EOS for *Re* has been discussed in detail in a recent study[8] where an overestimation of around 200 GPa was observed at a pressure of 430 GPa. Therefore our EOS plots in Figure 7 reaffirm this overestimation at ultra-high pressures. As far as the comparison of *Ta* EOS labeled as Nonhydrostatic I in Figure 7 with the shock compression is concerned, overall the agreement is reasonable. Our static bulk modulus measurement for *Ta* of $K_0$ =186.6 GPa is within 1.5% of the shock compression value of 189.4 GPa and is within our experimental errors. On the other hand, our static first pressure derivative of bulk modulus $K'_0$ = 4.36 is 10 % higher than shock compression value of 3.90 which is a significant difference. As a result, the shock compression EOS begins to diverge from the static EOS above 50 GPa and is softer; i.e., results in a lower pressure for a given volume compression of *Ta*. In Figure 7, we also show the extrapolation of ultrasonic EOS based on $K_0$ = 194 GPa and $K'_0$ = 3.83 in conjunction with equation (1). The shock EOS and ultrasonic EOS show overlap to the highest volume compression compression $V/V_0$ = 0.581. The insert in Figure 7 shows comparison of quasi-hydrostatic and non-hydrostatic EOS for *Ta* to 80 GPa. The quasi-hydrostatic fit yields a bulk modulus value $K_0$ = 201 GPa that is higher than the non-hydrostatic value of 186.6

GPa and hence the quasi-hydrostatic curve is slightly stiffer compared to non-hydrostatic case as shown in the insert in Figure 7. However, the maximum difference in pressure between the quasi-hydrostatic and non-hydrostatic EOS is only 2.5 GPa at 80 GPa. This difference of 2.5 GPa between the quasi-hydrostatic and non-hydrostatic pressure is within the maximum differental stress or the yield stength of 4 GPa for *Ta* at a pressure of 80 GPa[21].

## CONCLUSIONS

We have carried out room temperature equation of state measurements on *Ta* to 310 GPa using *Re* and *Au* as pressure standards under both quasi-hydrostatic and non-hydrostatic environments. The *Ta* metal was observed to be stable in the body-centered-cubic phase to a volume compression V/V0 = 0.581. The present study provides comparison of EOS of *Ta* using two different claibration for *Re* pressure standard and observed a significant overestimation of pressure in one case.and subsequently omitted that calibration for comparison with the shock data. The measured static pressure EOS to 310 GPa is in general agreement with shock data, however, shock EOS tend to be softer above 50 GPa. The difference between the quasi-hydrostatic and the non-hydrostatic EOS is 2.5 GPa at 80 GPa which is within the measured yield strength or maximum differential stress of *Ta* at this pressure.

## ACKNOWLEDGEMENTS

We would like to acknowledge support from the U.S. National Science Foundation (NSF) under Metals and Metallic Nanostructures program Grant No. DMR-1608682. Los Alamos National Laboratory (LANL) is operated by Triad National Security, LLC for the DOE-NNSA under Contract No. 89233218CNA000001. NV, EKM, JSP, and BTS acknowledge funding support from LANL Science Programs 1 and 2. Portions of this work were performed at HPCAT (Sector 16), Advanced Photon Source (APS), Argonne National Laboratory. HPCAT operations are supported by DOE-NNSA's Office of Experimental Sciences. The Advanced Photon Source is a U.S. Department of Energy (DOE) Office of Science User Facility operated for the DOE Office of Science by Argonne National Laboratory under Contract No. DE-AC02-06CH11357. We also thank Dr. Richard Marten at the University of Alabama – Tuscaloosa for his assistance in the FIB machining of toroidal anvils, Sergey Tkachev of GSECARS for the neon gas-loading, and HPCAT 16-BM-D beamline support from Dmitry Popov and Changyong Park.

**REFERENCES:**


1. N. Dubrovinskaia, L. Dubrovinsky, N. A. Solopova, A. Abakumov, S. Turner, M. Hanfland, E. Bykova, M. Bykov, C. Prescher, V. B. Prakapenka, S. Petitgirard, I. Chuvashova, B. Gasharova, Y-L. Mathis, P. Ershov, I. Snigireva and A. Snigirev, "Terapascal static pressure generation with ultrahigh yield strength nanodiamond," Science Advances **2**, e1600341 (2016).
2. L. Dubrovinsky, N. Dubrovinskaia, E. Bykova, M. Bykov, V. Prakapenka, C. Prescher, K. Glazyrin, H.-P. Liermann, M. Hanfland, M. Ekholm, Q. Feng, L. V. Pourovskii, M. I. Katsnelson, J. M. Wills, I. A. Abrikosov, I.A., "The most incompressible metal osmium at static pressures above 750 gigapascals," Nature **525**, 226-229 (2015).
3. L. Dubrovinsky, N. Dubrovinskaia, V. B. Prakapenka and A. M. Abakumov, "Implementation of micro-ball nanodiamond anvils for high-pressure studies above 6 Mbar," Nat. Commun.**3**, 1163 (2012).
4. Y. K. Vohra, G. K. Samudrala, S. L. Moore, J. M. Montgomery, G. M. Tsoi and N. Velisavljevic, " High pressure studies using two-stage diamond micro anvils grown by chemical vapor deposition", High Pressure Research **35**, 282 (2015).
5. G. K. Samudrala, S. L. Moore, N. Velisavljevic, G. M. Tsoi, P. A. Baker, and Y. K. Vohra, "Nanocrystalline diamond micro-anvil grown on single crystal diamond as a generator of ultra-high pressures", American Institute of Physics Advances **6**, 095027 (2016).
6. Samuel L. Moore, Gopi K. Samudrala, Shane A. Catledge, and Yogesh K. Vohra, "Rapid Growth of Nanocrystalline Diamond on Single Crystal Diamond for Studies on Materials under Extreme Conditions", Scientific Reports **8**, 1402 (2018).
7. S. S. Lobanov, V. B. Prakapenka, C. Prescher, Z. Konôpková, H-P. Liermann, K. L. Crispin, C. Zhang, and A. F. Goncharov "Pressure , stress , and strain distribution in the double-stage diamond anvil cell," J. Appl. Phys. **118**, 035905, (2015).
8. T. Sakai, T. Yagi, H. Ohfuji, T. Irifune, Y. Ohishi, N. Hirao, Y. Suzuki, Y. Kuroda, T. Asakawa, and T. Kanemura, "High-pressure generation using double stage micro-paired diamond anvils shaped by focused ion beam," Rev. Sci. Instrum. **86**, 033905 (2015).
9. T. Sakai, T. Yagi, T. Irifune, H. Kadobayashi, N. Hirao, T. Kunimoto, H. Ohfuji, S. Kawaguchi-Imada, Y. Ohishi, S. Tateno and K. Hirose "High pressure generation using double-stage diamond anvil technique: problems and equations of state of rhenium," High Pressure Research **38**, 107-119 (2018).
10. A. Dewaele, P. Loubeyre, F. Occelli, O. Marie, and M. Mezouar, "Toroidal diamond anvil cell for detailed measurements under extreme static pressures", Nature Communications **9**, 2913 (2018).
11. Z. Jenei, E. F. O'Bannon, S. T. Weir, H. Cynn, M. J. Lipp, and W. J. Evans, "Single crystal torroidal anvils for high pressure experiments beyond 5 megabar", Nature Communications 9, 3563 (2018).

12. S. Anzellini, A. Dewaele, F. Occelli, P. Loubeyre, and M. Mezouar, “Equation of state of rhenium and application for ultra high pressure calibration”, J. Appl. Phys. **115**, 043511 (2015).
13. P.I. Dorogokupets and A. Dewaele, “Equations of state of MgO, Au, Pt, NaCl-B1, and NaCl-B2: Internally consistent high-temperature pressure scales,” High Pressure Research 27, (2007).
14. Prescher, C., Prakapenka, V.B. “DIOPTAS : a program for reduction of two-dimensional X-ray diffraction data and data exploration”. High Press. Res. 35:3, 223–230 (2015).
15. Toby, B. H., & Von Dreele, R. B. "GSAS-II: the genesis of a modern open-source all purpose crystallography software package". *Journal of Applied Crystallography*, **46**(2), 544-549 (2013).
16. P. Vinet, J. Ferrante, J. H. Rose, and J. R. Smith, “Compressibility of solids”, J. Geophys. Res. **92**, 9319 (1987).
17. R. G. McQueen, S. P. Marsh, J. W. Taylor, J. N. Fritz, and W. J. Carter, *High Velocity Impact Phenomenon* (Academic, New York, 1970).
18. H. Cynn and C. Yoo, “Equation of state of tantalum to 174 GPa”, Phys. Rev. **B 59**, 8526 (1999).
19. A. Dewaele P. Loubeyre, and M. Mezouar, “Refinement of equation of state of tantalum”, Phys. Rev. **B 69**, 092106 (2004).
20. K. Katahara, M. Manghnani, and E. Fisher, “Pressure derivatives of the elastic moduli of niobium and tantalum”, J. Appl. Phys. **47**, 434 (1976).
21. A. Dewaele and P. Loubeyre, “Mechanical properties of tantalum under high pressure”, Phys. Rev. **B 72**, 1341016 (2005).

**Table 1:** Experimental conditions, pressure standards , and equation of state fit parameters in the present studies on *Ta* and comparison with the ultrasonic data. All the fit parametrs in this study are based on the Rydberg-Vinet equation of state[16].

| Experimental Description | Pressure Marker | Pressure Range (GPa) | Bulk Modulus $K_0$ (GPa) | Pressure Derivative $K'_0$ | Reference |
|---|---|---|---|---|---|
| Non-hydrostatic I using Anzellini *et al*[12] EOS for *Re* | Rhenium | 0 - 310 | 186.6±2.0 | 4.36±0.05 | This study |
| Non-hydrostatic II using Dubrovinsky *et al*[3] EOS for *Re* | Rhenium | 0 – 422 | 166.1±1.4 | 6.05±0.01 | This study |
| Shock Compression | - | 0 – 230 | 189.4±1.8 | 3.90±0.05 | Fitted data from Reference 17 |
| Quasi-hydrostatic (neon-medium) | Gold | 0-80 | 201.0±2.4 | 3.21±0.11 | This study |
| Ultrasonic Data | - | 0-0.5 | 194 | 3.83 | Reference 20 |

**FIGURE CAPTIONS:**

**Figure 1:** Scanning Electron Microscopy (SEM) (a) Side-view of the starting beveled diamond anvil. (b) Top-view of the FIB machined toroidal anvil with a central flat region of 16 microns and outer regions of 40 and 65 microns in diameter. (c) Close-up side-view of the toroidal shape of the diamond anvil showing a groove depth of 2.6 microns.This toroidal anvil achieved a peak pressure of 265 GPa.

**Figure 2:** Scanning Electron Microscopy (SEM) (a) image of starting diamond culet before FIB milling. (b) SEM image after milling is complete with a central flat region of 8 microns and outer regions of 20 and 35 microns in diameter. (c) Close-up side-view of the toroidal shape of the diamond anvil with a groove depth of 5 microns. This toroidal anvil achieved a peak pressure of 310 GPa.

**Figure 3:** (a) X-ray diffraction pattern and Rietveld refinement difference curve for tantalum-rhenium (*Ta-Re*) mixture in a toroidal diamond anvil cell at 265 GPa. The *Ta*-diffraction peaks are indexed to a body-cented-cubic phase while the *Re*-diffraction peaks are indexed to a hexagonal close-packed phase. (b) X-ray diffraction image of *Ta-Re* obtained by the Pilatus 1M detector at 265 GPa. The vertical lines labeled with an asterisk(*) indicate *Ta* diffraction while the *Re* diffraction lines shows spottiness or preferred orientation effects. The X-ray wavelength was $\lambda$=0.4066 Å.

**Figure 4:** 2-D x-ray transmission scan of ±20 micron range on toroidal anvil surface at a peak pressure of 310 GPa for the anvil shown in Figure 2. The maximum transmission area indicated by a circle at the center represents the toroidal anvil central flat of 8 microns in diameter. The x-ray transmission intensity profile within the toroidal region of 35 microns shows a very symmetric shape to the highest pressure.

**Figure 5:** The measured quasi-hydrostatic equation of state of *Ta* to 80 GPa using *Au* as a pressure marker and neon as a pressure medium. The solid curve is a Rydberg-Vinet[16] equation of state fit to the data with fit parameters described in Table 1.

**Figure 6:** The measured non-hydrostatic equation of state of *Ta* to 310 GPa ($V/V_0 = 0.581$) using *Re* as a pressure marker and using equation of state parameters by Anzellini *et al*[12]. The error bars are shown for only one data point for clarity of the goodness of fit. The solid curve is a Rydberg-Vinet[16] equation of state fit to the data with fit parameters described in Table 1 (Non-hydrostatic I).

**Figure 7:** The comparison of measured equation of state of *Ta* with two different EOS of *Re* by Anzellini *et al*[12] and Dubrovinsky *et al*[3] (Non-hydrostatic I and Non-hydrostatic II). The experimental static EOS for *Ta* is also compared with the ambient temperature isotherm derived from the shock data[17] and the extrapolation of ultrasonic EOS[20]. The ultrasonic EOS and shock EOS show overlap up to highest volume compression compression $V/V_0$ = 0.581. The fit parameters for all the five curves are described in Table 1. The insert shows the comparison between Quasi-hydrostatic and Non-hydrostatic-I EOS of *Ta* to 80 GPa.

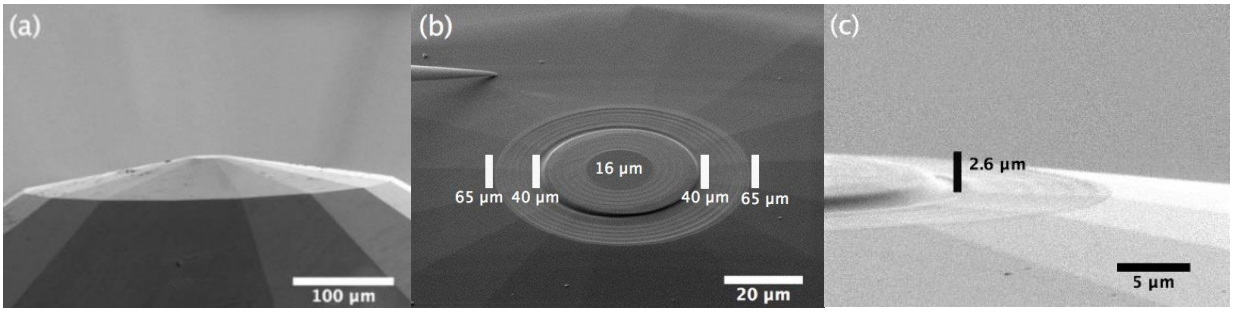


**FIGURE 1**

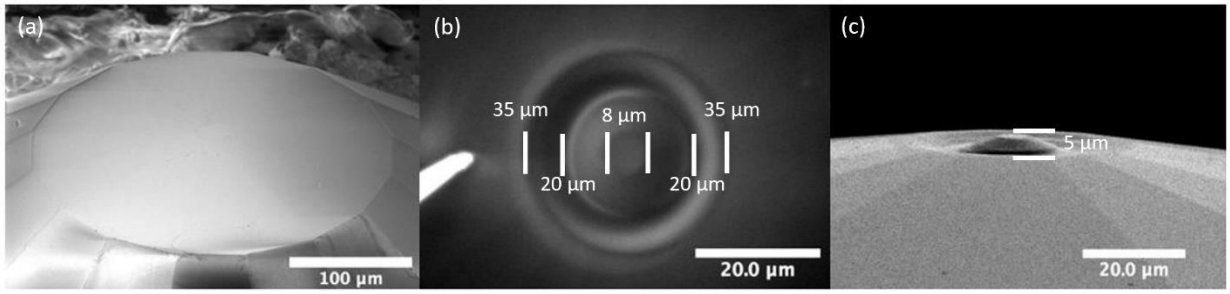


**FIGURE 2**

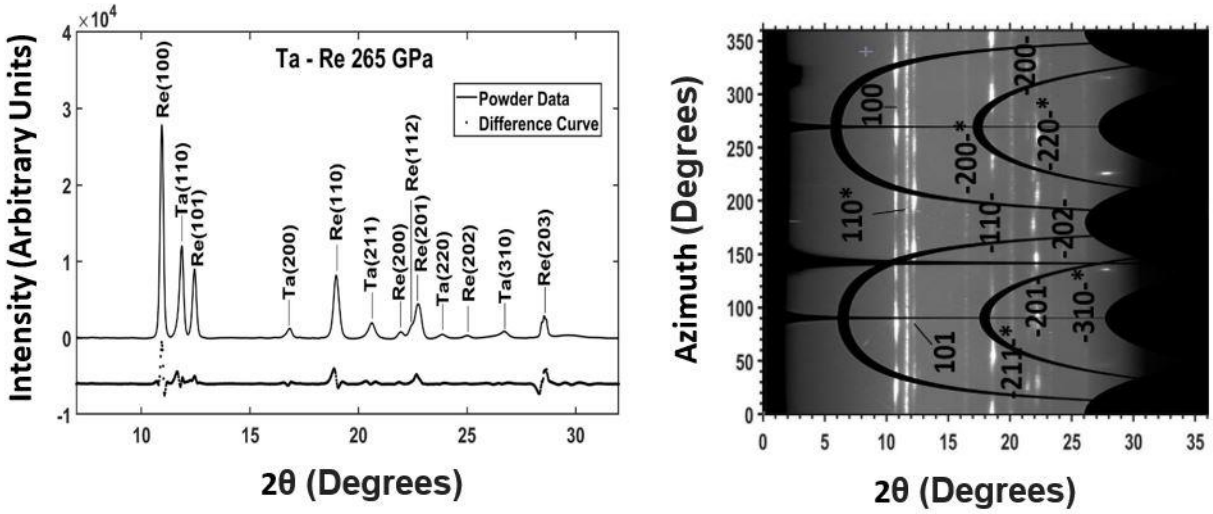
Ta - Re 265 GPa
Powder Data
Difference Curve
Intensity (Arbitrary Units)
2θ (Degrees)
Re(100)
Ta(110)
Re(101)
Ta(200)
Re(110)
Ta(211)
Re(200)
Re(112)
Re(201)
Ta(220)
Re(202)
Ta(310)
Re(203)
Azimuth (Degrees)
2θ (Degrees)
100
110*
-200-*
-110-
-200-
-220-*
-202-
101
211*
-201
-310-*

(a) (b)

**FIGURE 3**

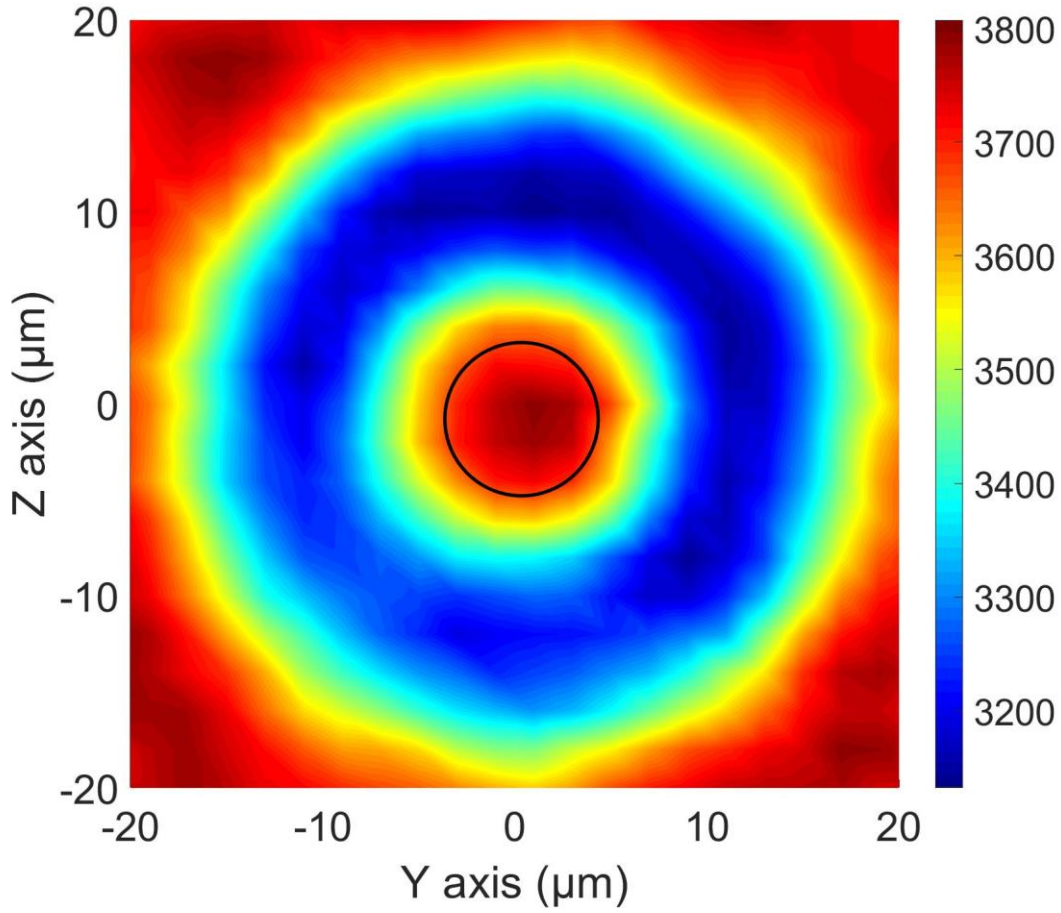
20
10
0
-10
-20
Z axis (μm)
-20
-10
0
10
20
Y axis (μm)
3800
3700
3600
3500
3400
3300
3200

**FIGURE 4**

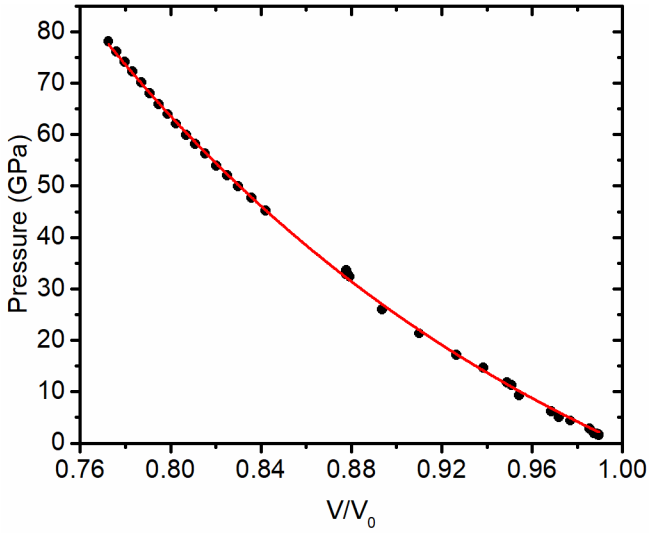
Pressure (GPa)
80
70
60
50
40
30
20
10
0
0.76
0.80
0.84
0.88
0.92
0.96
1.00
V/V0

**FIGURE 5**

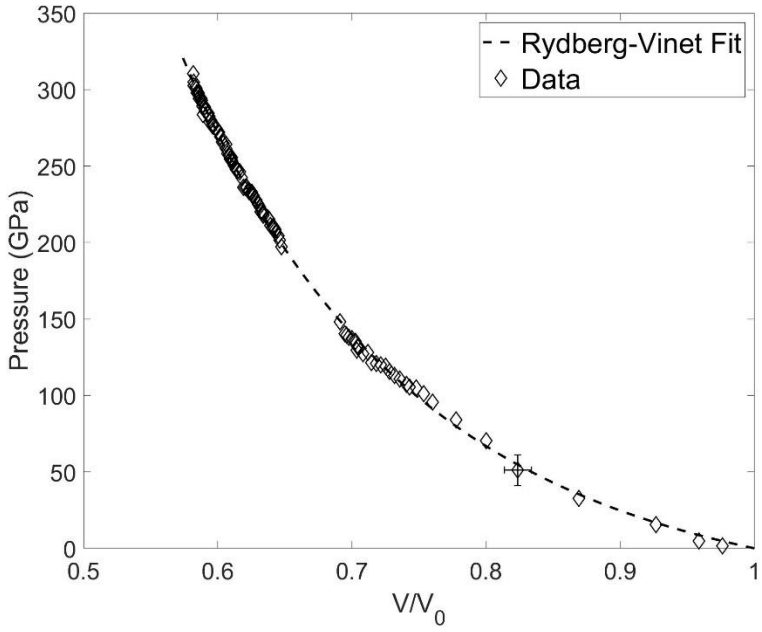
Rydberg-Vinet Fit
Data
Pressure (GPa)
V/V0
350
300
250
200
150
100
50
0
0.5
0.6
0.7
0.8
0.9
1

**FIGURE 6**

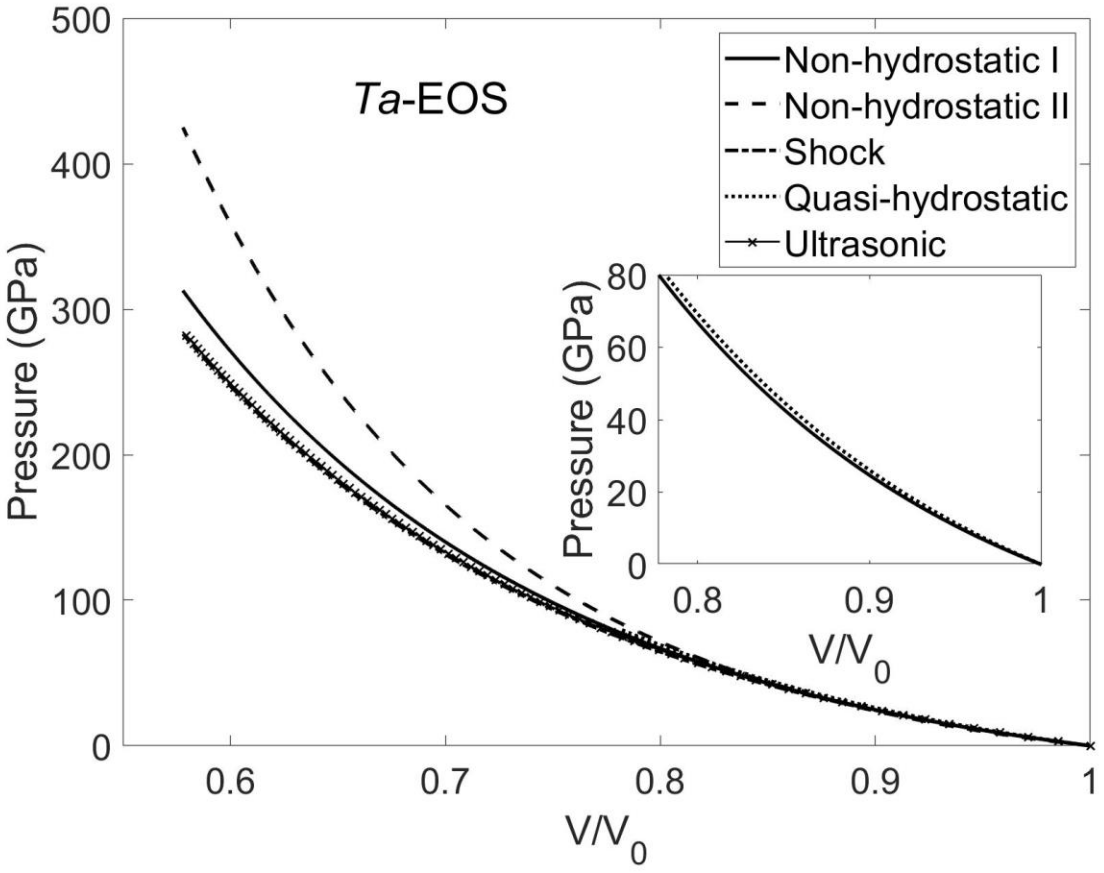
Ta-EOS
Non-hydrostatic I
Non-hydrostatic II
Shock
Quasi-hydrostatic
Ultrasonic
Pressure (GPa)
V/V0
500
400
300
200
100
0
0.6
0.7
0.8
0.9
1
80
60
40
20
0

**FIGURE 7**